Proceedings of the ASME 2023
International Design Engineering Technical Conferences and
Computers and Information in Engineering Conference
IDETC-CIE2023
August 20-23, 2023, Boston, Massachusetts

DETC2023-117069

OCEAN WAVE ENERGY CONVERSION WITH A SPAR-FLOATER SYSTEM USING A NONLINEAR INERTER PENDULUM VIBRATION ABSORBER

Aakash Gupta, Wei-Che Tai
Department of Mechanical Engineering
Michigan State University
East Lansing, Michigan 48824
e-mail: guptaaa3@msu.edu
e-mail: taiweich@msu.edu

ABSTRACT

The inerter pendulum vibration absorber is connected with a power take-off mechanism (called IPVA-PTO) to study its wave energy conversion potential. The resulting IPVA-PTO system is integrated between a spar and a floater (torus) using a ball-screw mechanism. The hydrodynamic stiffness, added mass and radiation damping effects on the spar-floater system are characterized using boundary element method via Ansys Aqwa. It has been observed that a 1:2 internal resonance between the spar-floater system and the pendulum is responsible for nonlinear energy transfer between the two systems. This nonlinear energy transfer occurs when the primary harmonic solution of the system becomes unstable, and a secondary solution emerges in the system characterized by harmonics of frequency half the excitation frequency. As a result of this energy transfer, the vibration of the spar-floater system is suppressed, and the energy is transferred to the pendulum. The focus of this paper is to analyze this 1:2 internal resonance phenomenon near the resonant frequency of the spar. The IPVA-PTO system, when integrated with the spar-floater system, is compared to a linear coupling between the spar and the floater in terms of the response amplitude operator (RAO) of the spar and the energy conversion capability defined by the capture width of the energy converter.

1 Introduction

Wave energy converters (WECs) are being integrated with offshore floating platforms as they can share infrastructure, equipment, mooring and anchoring systems, and survey and monitoring methods [1]. The reason for this integration getting popular is because the cost of installation and maintenance accounts for 40-50% cost in wave energy projects [2]. Further, the oil and gas industry has been investigating the feasibility of converting mature offshore platforms into renewable energy hubs by mounting WECs to the platforms [3]. The WECs can directly supply electricity to the platforms to further lower the cost of wave energy [4].

Offshore floating platforms are worldwide operating in deep water areas for oil and gas production [5] and providing the foundation for floating wind turbines [6]. Specifically, spar platforms establish the buoyancy and stability on a long and slender cylinder that goes deep below the water surface, thereby having good hydrodynamic response/stability and large water depths (600–2500 meters for oil spar platforms in the Gulf of Mexico [7]). On the other hand, heaving WECs convert the relative heave motion between oscillating bodies into electricity and have a high wave energy conversion efficiency when operating at resonance [8]. As the wave energy resources are more abundant in deep water than shallow water, it is reasonable to integrate WECs and spar platforms. Thus far, several researchers have studied the integration of a spar platform and different types of

heaving WECs [9–12]. Existing numerical studies [9,12] suggest that such integration can lead to a 7%–30% capture width ratio (hydrodynamic efficiency) of wave energy production, which is comparable with existing heaving WECs [13]. According to the scaling law in [13], heaving WECs of a larger diameter would have a higher capture width ratio. A typical spar platform in the Gulf of Mexico, e.g., the Horn Mountain, has a diameter of 30 meters (BSEE data [7]). If the spar-WEC integration in [9, 12] were scaled up to this diameter, the peak mean wave power in operational conditions would be 2.4–10 MW (current floating wind turbines have 5–MW wind power).

Although showing promising wave energy conversion, such integration does not assure good hydrodynamic response of the platform. Past studies have shown that the integration with heaving WECs amplifies the platform heave and pitch motion [9–11], and even cause Mathieu instability [14], which would aggravate fatigue of the mooring and riser systems and even lead to failure of the whole system [15, 16]. This deterioration of hydrodynamic response and stability can be explained as follows. Generally speaking, a spar platform has a 20–30 s heave natural period [17, 18] which is far away from typical incident wave periods (5–10 s [19]) to avoid large heave resonant response. On the other hand, traditional heaving WECs operate based on the basic principle of linear resonance, thereby having a natural period in heave close to a typical wave period to generate large heave resonant response and hence high-efficiency wave power production. When a heaving WEC is integrated with a platform, this large heave resonant response can give rise to large platform heave/pitch motions. In other words, wave power production and hydrodynamic response reduction are conflicting objectives in traditional linear WECs.

Recently, Gupta and Tai [20] integrated a nonlinear inerter pendulum vibration absorber (IPVA) with a heaving spar, and studied the hydrodynamic response and wave energy conversion of the integrated system. Specifically, the IPVA system was mounted between the spar and a fixed reference in a such way that the heave motion of the spar excites the IPVA. A power take-off is incorporated with the IPVA to convert the mechanical energy of the IPVA into electricity. They found that the pendulum of the IPVA can have resonant responses through 1:2 internal resonance while the spar's response is suppressed in the heave direction. This is due to a phenomenon of nonlinear energy transfer wherein the mechanical energy of the spar transfers to the pendulum via 1:2 internal resonance which has gained attention for wave energy conversion in recent years [21, 22]. Despite the promising results, it is difficult to create a fixed reference in the ocean. A more practical way is to incorporated the IPVA system in-between spar and a secondary body. For example, researchers have investigated a spar system that is integrated with a co-axial floater via linear power take-off [9, 11, 14, 23]. As the floater is directly mounted to the spar without additional mooring lines to a fixed reference, this methodology can be readily implemented in the ocean. Motivated by the practicality of the spar-floater system and the potential of the IPVA, this work integrates the spar and floater via the IPVA, and studies the hydrodynamic response and wave energy conversion of the integrated system. The PTO-integrated IPVA is referred to as IPVA-PTO hereinafter for brevity.

The rest of the paper is organized as follows. Section 2 talks about the design of the IPVA-PTO system and its integration with the spar-floater system. Section 3 derives the equation of motion considering the hydrodynamic effects on the system, whereas section 4 discusses the analysis of the IPVA-PTO system using harmonic balance formulation. Finally, section 5 talks about the efficacy of IPVA-PTO system when compared with a linear benchmark and section 6 concludes this study.

2 Design of the system

Figure 1a shows a spar and an annular floater floating in water connected by the IPVA-PTO system (Inerter Pendulum Vibration Absorber Power Take-Off system). For simiplicity, the spar and floater are constrained such that they can only move in the heaving (x) direction relative to the waterline. Figure 1b shows the IPVA system consisting of a lead screw, a carrier, a generator, and a pendulum vibration absorber. The nut of the lead screw is fixed to the floater while the screw is supported by a thrust bearing that is fixed to the spar through a housing. As a result, the relative heaving displacement $x_1 - x_2$ is converted into the angular displacement θ through $x_1 - x_2 = R\theta$, where $R = L/2\pi$, and L is the screw lead. The carrier is fixed to the screw such that they have the same angular displacement (θ) and hosts a sun gear. The pendulum pivots on a point of the carrier which is located at a distance of R_p from the carrier center, and is assumed to be a point mass for this study. The pendulum length is r and has an angular displacement ϕ with respect to the screw. The sun gear (mounted on the screw) hosts the rotor of the generator with the housing of the generator fixed to the spar. A planet gear is mounted on the shaft of the pendulum and meshes with the sun gear (hosting the generator's rotor). It can be shown that the rotational motion of the rotor of the generator with respect to its housing is given by $\theta - \phi$. Therefore, the instantaneous energy converted by the generator will be $c_e\left(\dot{\theta} - \dot{\phi}\right)^2$, where c_e denotes the electrical damping of the generator. Figure 1c shows the mathematical model of the system where k_1 and k_2 denote the hydrostatic stiffness in heave of the spar and floater, respectively, and M_1 and M_2 denote the spar and floater mass, respectively. Furthermore, the wave motion generates hydrodynamic forces f_1 and f_2, exciting the spar and floater, respectively. For the analysis in this study, the linear wave theory is assumed, and the derivation of the equation of motion is discussed in the next section.

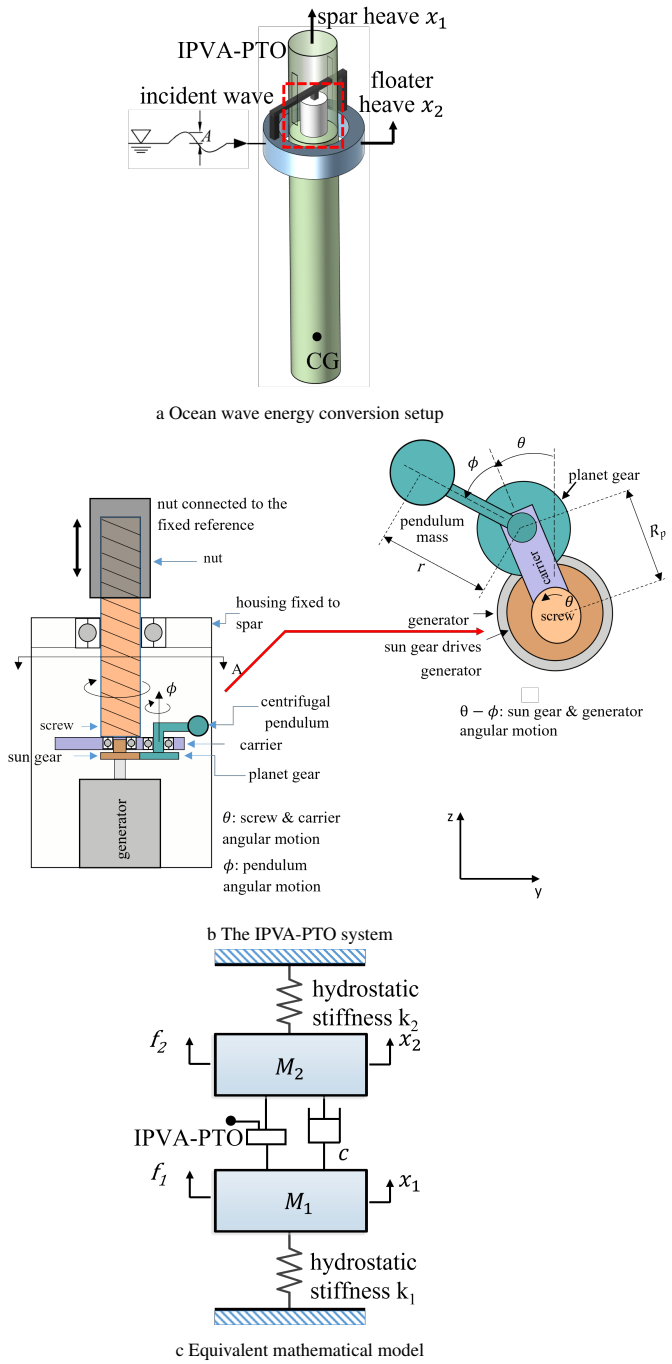

FIGURE 1: The IPVA-PTO system integrated in a Spar-Floater setup for wave energy conversion

3 Equations of motion

To facilitate deriving the equations of motion, the following coordinate transformation is employed:

$$\begin{aligned} x_2 &= R\psi \\ x_1 &= R(\theta+\psi) \end{aligned} \tag{1}$$

The Lagrange's equation is used to derive the equations of motion. The kinetic and potential energy of the system are determined, followed by the hydrodynamic coefficients and forces on the system. Finally, the virtual work due to the forces applied to the system is calculated and the equations of motion are derived and normalized. First, the sum T of the kinetic energy of the spar, floater and IPVA-PTO, and the sum V of the potential energy of the spar and the floater are given by

$$\begin{aligned} T &= \frac{1}{2}J_r\left(\dot\theta-\dot\phi\right)^2+\frac{1}{2}J_p\left(\dot\theta+\dot\phi\right)^2+\frac{1}{2}J_{bsc}\dot\theta^2 \\ &+ \frac{1}{2}m\left[\dot\theta^2\left(r^2+2rR_p\cos\phi+R_p^2\right)+r^2\dot\phi^2+2r\dot\theta\dot\phi\left(r+R_p\cos\phi\right)\right] \\ &+ \frac{1}{2}M_1\left(R\dot\theta+R\dot\psi\right)^2+\frac{1}{2}M_2R^2\dot\psi^2 \\ V &= \frac{1}{2}k_1(R\theta+R\psi)^2+\frac{1}{2}k_2R^2\psi^2 \end{aligned} \tag{2}$$

where k_1 and k_2 are hydrostatic stiffness of the spar and the floater, respectively. J_r, J_{bsc} and J_p are the moments of inertia of the generator's rotor, ball-screw-carrier assembly, and of the pendulum respectively. Next, the hydrodynamic coefficients of the spar and the floater subject to incident regular waves are determined by the linear wave theory, which assumes that the fluid is inviscid and irrotational [24]. Based on the linear wave theory, the hydrodynamic force on the spar and the floater consists of three components: Froude-Krylov force, diffraction force, and radiation force. The first two correspond to the incident wave field without and with the presence of the spar-floater system respectively, and the third term, radiation force, results from the oscillations of the spar-floater system.

The Froude-Krylov and diffraction force together determine the excitation force, while the radiation force gives rise to the added mass and radiation damping in the system [19, 24], which can be represented by the well-known Cummins' equation [25]:

$$F_{g,i} = -A_{\infty,i}\ddot{x}_i - \int_{\sigma=0}^{\infty} k_{R,i}(\sigma)\dot{x}_i(t-\sigma)\,d\sigma + \gamma F_i(t) \tag{3}$$

for $i = 1, 2$, where $F_{g,i}$ is the incoming wave force, $\gamma F_i = f_i$ is the excitation (Froude-Krylov and diffraction) force and γ is the wave amplitude. By virtual of the linear wave theory, $F_{g,i}$ is assumed to be sinusoidal. As a consequence, F_i is also sinusoidal with angular frequency Ω, equal to the frequency of the incoming wave. The radiation impulse response kernel, $k_{R,i}(\sigma)$ and the radiation infinite-frequency added mass, $A_{\infty,i}$, are related to the radiation frequency-dependent damping and added mass $B_{R,i}(\Omega)$

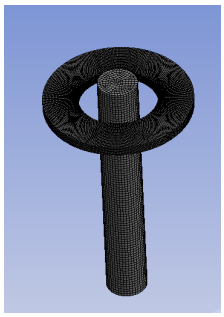

FIGURE 2: Ansys AQWA model for calculation of hydrodynamic coefficients

and $A_{R,i}(\Omega)$, through Ogilvie's relations [26]

$$B_{R,i}(\Omega) = \int_{\sigma=0}^{\infty} k_{R,i}(\sigma)\cos(\Omega\sigma)\,d\sigma,\ i=1,2,$$
$$A_{R,i}(\Omega) = A_{\infty,i} - \frac{1}{\Omega}\int_{\sigma=0}^{\infty} k_{R,i}(\sigma)\sin(\Omega\sigma)\,d\sigma,\ i=1,2, \quad (4)$$

with

$$A_{\infty,i} = \lim_{\Omega\to\infty} A_{R,i}(\Omega),\ i=1,2, \quad (5)$$

Here, the hydrodynamic coefficients, Froude-Krylov and diffraction force are determined using Ansys AQWA. For the calculation of the hydrodynamic coefficients, the spar-floater system was modeled together in AQWA, but not connected to each other physically, though they influenced each other's hydrodynamics. A convergence test was performed like previously illustrated in [27] to match the published results in [28]. After verifying the Ansys model, the same setting is adopted to simulate the spar-floater system. The height of the spar is taken as 1.06m with a draft of 0.96m (the height below the surface of the water), and a diameter of 0.16m, corresponding to the 1:100 scale sparD model with water depth of 3m as described in [29]. The floater, on the other hand, is an annulus with a depth of 0.02m with inner diameter of 0.317m and outer diameter of 0.595m. Fig. 2 shows the mesh of the system used for analysis and Fig. 3 shows the added mass, radiation damping, and excitation force obtained using Ansys for both the spar and the floater.

Next we obtain the virtual work by different terms in the system. The total virtual work of the system can be defined as

$$\delta W = \delta W_{AM} + \delta W_{RD} + \delta W_F + \delta W_D \quad (6)$$

where δW_{AM}, δW_{RD}, δW_F and δW_D are the virtual works due to the added mass, radiation damping, excitation force and mechanical damping, respectively, and are calculated as follows

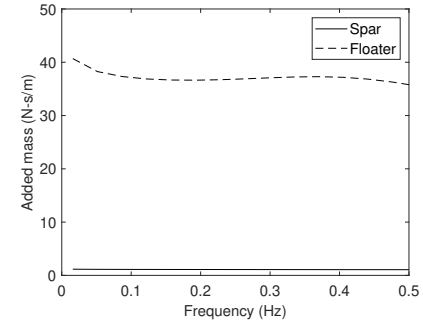

a Added mass

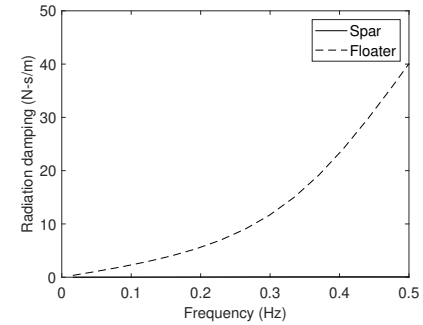

b Radiation damping

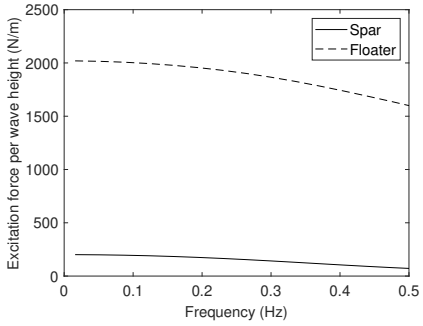

c Diffraction and Froude-Krylov force

FIGURE 3: Added mass, radiation damping, and diffraction and Froude-Krylov force for spar and floater

$$\delta W_{AM} = -A_{\infty,1}\left(\ddot{\theta}+\ddot{\psi}\right)R^2(\delta\theta+\delta\psi) - A_{\infty,2}R^2\ddot{\psi}\delta\psi,$$
$$\delta W_{RD} = -\left[\int_0^{\infty} R^2\kappa_1(\tau)\left(\dot{\theta}(t-\tau)+\dot{\psi}(t-\tau)\right)d\tau\right] \times(\delta\theta+\delta\psi) - \left[\int_0^{\infty} R^2\kappa_2(\tau)\,\dot{\psi}(t-\tau)\,d\tau\right]\delta\psi, \quad (7)$$
$$\delta W_F = Rf_1(\delta\theta+\delta\psi) + Rf_2\delta\psi,$$
$$\delta W_D = -cR^2\dot{\theta}\delta\theta - c_e\left(\dot{\theta}-\dot{\phi}\right)\delta(\theta-\phi), \quad (8)$$

where c_e is the electrical damping due to the generator, and c is

the mechanical damping between the spar and the floater. The damping in the pendulum is assumed to be significantly less than the electrical damping and is ignored in the analysis. Using the above expressions, the θ, ϕ and ψ contributions due to virtual work into the equations of motion can be obtained. After substituting the kinetic energy, potential energy, and the virtual work, and using the following normalization parameters

$$\begin{aligned}
&\eta_g = \frac{J_r}{M_1R^2},\ \mu_F = \frac{M_1}{M_2},\ \eta = \frac{r}{R_p},\ \omega_0 = \sqrt{\frac{k_1}{M_1}},\\
&\omega_2 = \sqrt{\frac{k_2}{M_2}},\ \mu_r = \frac{mR_p^2}{M_1R^2},\ \mu_{bsc} = \frac{J_{bsc}}{M_1R^2},\ \ \mu_p = \frac{J_p}{M_1R^2},\\
&\omega = \frac{\Omega}{\omega_0},\ \omega_r = \frac{\omega_2}{\omega_0}, \tau = \omega_0 t,\ \eta = \frac{r}{R_p},\ \xi = \frac{c}{2\omega_0 M_1},\\
&\xi_e = \frac{c_e}{2\omega_0 M_1R^2},\ ()' = \frac{d()}{d\tau},\ f_{e,1} = \frac{f_1}{\omega_0^2 M_1 R},\\
&f_{e,2} = \frac{f_2}{\omega_0^2 M_1 R},\ \mu_{A\infty,1} = \frac{A_{\infty,1}}{M_1},\ \mu_{A\infty,2} = \frac{A_{\infty,2}}{M_1},
\end{aligned} \tag{9}$$

the following equation of motion is obtained

$$\mathbf{M}\mathbf{x}'' + \mathbf{C}\mathbf{x}' + \mathbf{K}\mathbf{x} + \boldsymbol{\mathcal{R}}(\dot{\mathbf{x}}) = \mathbf{F}, \tag{10}$$

where

$$\begin{aligned}
\mathbf{M} &= \begin{pmatrix} a_{11} & a_{12} & a_{13} \\ a_{12} & a_{22} & 0 \\ a_{13} & 0 & a_{33} \end{pmatrix},\ \mathbf{C} = \begin{pmatrix} 2(\xi+\xi_e) & 0 & -2\xi_e \\ 0 & 0 & 0 \\ -2\xi_e & 0 & 2\xi_e \end{pmatrix},\\
\mathbf{K} &= \begin{pmatrix} 1 & 1 & 0 \\ 1 & 1+\mu_F\omega_r^2 & 0 \\ 0 & 0 & 0 \end{pmatrix},\ \boldsymbol{\mathcal{R}}(\dot{\mathbf{x}}) = \frac{1}{M_1\omega_0^2}\begin{pmatrix} r_1 \\ r_1+r_2 \\ 0 \end{pmatrix},\\
\mathbf{F} &= \begin{pmatrix} f_{e,1} + 2\eta\mu_r\theta'\phi'\sin\phi + \eta\mu_r\phi'^2\sin\phi \\ f_{e,1}+f_{e,2} \\ -\eta\mu_r\theta'^2\sin\phi \end{pmatrix}
\end{aligned} \tag{11}$$

where

$$\begin{aligned}
a_{11} &= \eta^2\mu_r + \mu_{bsc} + \mu_r + \mu_p + 2\eta\mu_r\cos\phi + 1 + \eta_g + \mu_{A\infty,1}\\
a_{12} &= 1+\mu_{A\infty,1},\ a_{13} = -\eta_g + \mu_p + \eta^2\mu_r + \eta\mu_r\cos\phi,\\
a_{22} &= \mu_F + 1 + \mu_{A\infty,1} + \mu_{A\infty,2},\ a_{33} = \mu_p + \eta^2\mu_r + \eta_g,\\
r_1 &= \int_0^\infty \kappa_1(\tau)\left[\theta'(t-\tau) + \psi'(t-\tau)\right]d\tau,\\
r_2 &= \int_0^\infty \kappa_2(\tau)\,\psi'(t-\tau)\,d\tau
\end{aligned} \tag{12}$$

4 Analysis of the IPVA-PTO system

Following the idea laid out in [20,27], the boundary of parametric instability where the primary harmonic solution (corresponding to 1:1 resonance of the system) of the system becomes unstable can be obtained. Since the spar-floater system (without considering the IPVA-PTO) has two degrees of freedom, we will have two natural frequencies. For the current study, we analyze the system near its first natural frequency. To that end, the harmonic balance method with alternating frequency time method (AFT) and Floquet theory are used as explained in [27].

As has been reported previously in [20,27], the instability in the primary solutions for the system gives rise to period doubling bifurcations and the secondary solutions (with harmonics of frequency $\frac{\omega}{2}$ along with ω) emerges in the response. The emergence of secondary solution is a result of period-doubling bifurcation (1:2 internal resonance in this case) in the system, where the primary resonance (1:1 resonance) of the system becomes unstable. This is accompanied by nonlinear energy transfer between the primary system and the pendulum. Therefore, the bifurcation tracking algorithm developed in [20] with modified AFT method proposed in [27] is used to obtain the period-doubling bifurcation boundary of the current system. Fig. 4 shows the boundary of period-doubling bifurcation with wave height on the y-axis and wave frequency on the x-axis for parameters listed in Table 1. As has been previously observed in [20, 27], below this boundary, the primary harmonic response of the system is stable, and above this boundary, it becomes unstable giving rise to a secondary solution which contains harmonics of half the excitation frequency (incoming wave frequency in this study). To verify this behavior, the hydrodynamic response with two wave heights ($\times1$ and $\times2$ in Fig. 4) is simulated using the ode45 solver in Matlab along with the state-space method described in [27]. Fig. 5 and Fig. 6 plot the time series response and fast Fourier transform (FFT) of the pendulum motion ϕ with the wave height and wave frequency corresponding to points $\times1$ and $\times2$ in Fig. 4. For the FFT plots, the x-axis parameter ($\hat{\omega}$) is the angular frequency normalized with respect to the wave angular frequency, which means that $\hat{\omega} = 1$ corresponds to the primary solution. As seen from Fig. 5 and Fig. 6, below the stability boundary (at point $\times1$), the solution is strictly primary, whereas above the boundary (at point $\times2$), the motion of the pendulum contains harmonics of frequency $\frac{\omega}{2}$. Next, to see the nonlinear energy transfer in action, we investigate the response of the system for wave heights below and above the boundary in the next section.

5 Discussion

From the stability boundary, it is expected that for the frequency range within which the wave height is above the stability boundary, there will be nonlinear energy transfer between the spar-floater system and the pendulum due to 1:2 internal resonance [20]. Thus, to benchmark this system, we define a lin-

Parameter	Value
ξ_e	0.02
ξ	0.05
μ_r	0.4
η	0.4
$\mu_{A\infty,1}$	0.0554
$\mu_{A\infty,2}$	0.6381
ω_r	6.928
ω_0	3.20 rad/s
η_g	0.01
μ_p	0.02
μ_{bsc}	0.04
μ_F	0.2097

TABLE 1: Parameters for the IPVA system

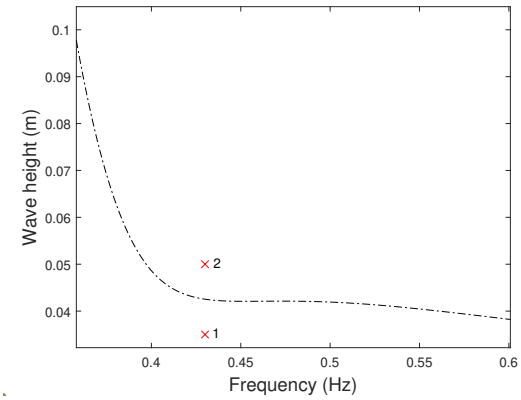

FIGURE 4: Stability boundary for the primary harmonics of the system

ear system and compare two measures of both the IPVA-PTO and the linear system, which are the response amplitude operator (RAO) of the spar and the normalized capture width. The RAO of the spar is defined as the heaving amplitude of the spar per unit wave height. On the other hand, the normalized capture width is defined as the value of the energy converted by the IPVA-PTO divided by the maximum energy converted by the linear system. For a fair comparison, we define linear system as the system with the pendulum locked at a position such that the peak frequency of the RAO for the linear system matches that of the IPVA-PTO system. Both the linear system and the IPVA-PTO

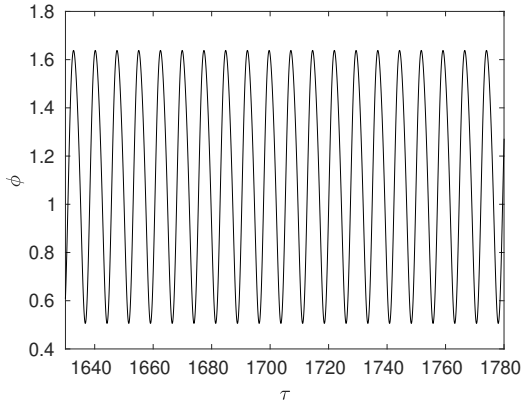

a Time series of the pendulum motion at point 1

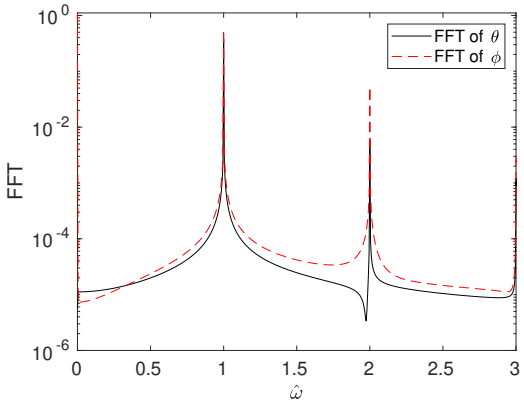

b FFT of the pendulum motion at point 1

FIGURE 5: Time series and FFT of the pendulum motion

system are solved using ode45 in Matlab. The integration kernel in the equation of motion is evaluated using an impulse to state-space converter function described in [27, 30]. The parameters used for the simulation are shown in Table 1, with the exception of electrical damping ratio of the linear system $\xi_{e,l}$, which is mentioned in the figure caption for various cases. The wave height is fixed to 6 cm, which is above the stability boundary for a range of frequencies. Since, we would like to convert the maximum energy possible, we first find the optimal linear electrical damping by solving the linear system and optimizing for the converted energy. It was found that $\xi_{e,l} = 0.0701$, and it can be observed from Fig. 7, that the IPVA-PTO system outperforms the linear system in terms of both the RAO and the maximum normalized capture width to that of the linear system. It should also be noted that the IPVA-PTO system has a broader bandwidth. For a fairer comparison, we can choose the electrical damping of the linear system such that the maximum RAO matches for both the system, and compare the normalized captured width or the measure of wave energy conversion. To that end, we fix $\xi_{e,l}$ to 0.115 and compare the results as shown in Fig. 8. As can be observed, the maximum normalized capture width of IPVA-PTO

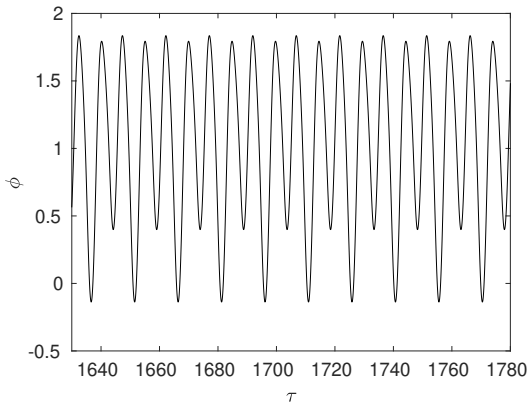

a Time series of the pendulum motion at point 2

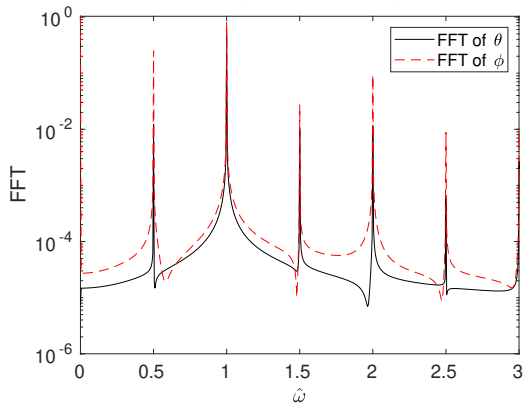

b FFT of the pendulum motion at point 2

FIGURE 6: Time series and FFT of the pendulum motion

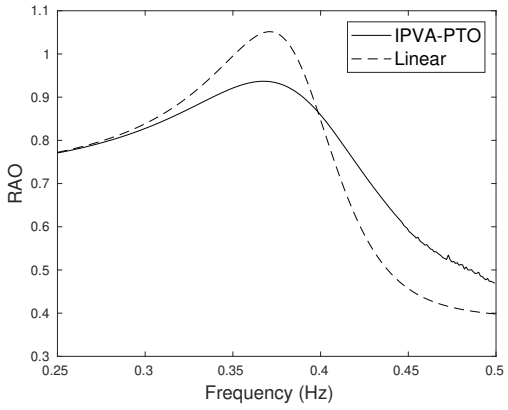

a RAO

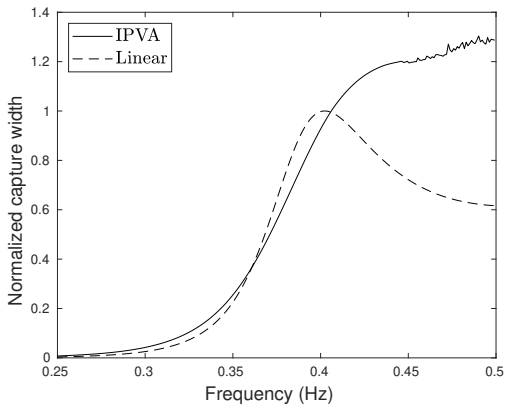

b Normalized capture width

FIGURE 7: Comparison between RAO and normalized capture width of the IPVA-PTO and the linear system for a wave height of 6 cm and $\xi_e = 0.0701$, optimized for maximizing energy converted (others parameters are shown in table 1)

is higher than that of the linear system by around a factor of 1.35 when the maximum RAO is the same. This can be attributed to the nonlinear energy transfer between the primary system and the pendulum.

6 Conclusion

This study analyzes the incorporation of the IPVA system [20] into a floating spar-floater system for wave energy conversion. The hydrodynamic response and wave energy conversion of the integrated system when the wave frequency is near the spar resonance frequency are investigated in terms of numerical simulations. A harmonic balance method is used to determine the boundary of period-doubling bifurcation in the parameter plane of wave height and wave frequency. According to the boundary, one can determine a combination of the wave height and frequency such that 1:2 internal resonance occurs to the IPVA system. It is observed that the 1:2 internal resonance is associated with a nonlinear energy transfer phenomenon similar to that observed in [20, 27]. It is also shown that because of this energy transfer phenomenon, the IPVA-PTO system is shown to achieve a higher capture width when the maximum RAOs are equal, when compared with its linear counterpart.

ACKNOWLEDGMENT

This material is based upon work supported by the National Science Foundation under Grant No. 2127495. Any opinions, findings, and conclusions or recommendations expressed in this material are those of the authors and do not necessarily reflect the views of the National Science Foundation.

REFERENCES

[1] Nguyen, H., Wang, C., Tay, Z., and Luong, V., 2020. "Wave energy converter and large floating platform integration: A review". *Ocean Engineering,* **213**, p. 107768.

[2] Bedard, R., Hagerman, G., Previsic, M., Siddiqui, O., Thresher, R., and Ram, B., 2005. "Final summary report, project definition study, offshore wave power feasi-

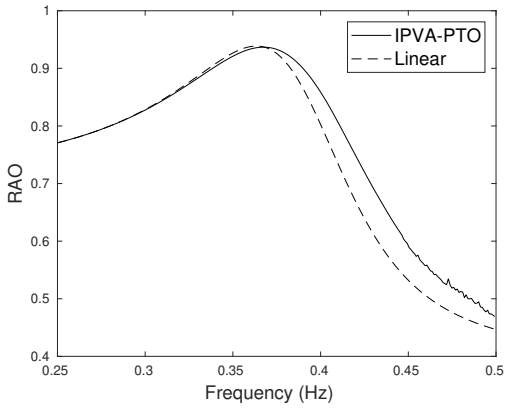

a RAO

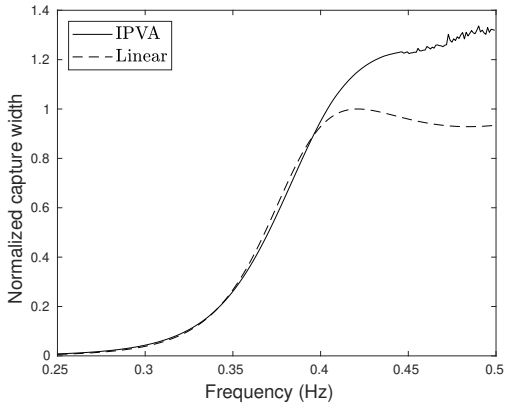

b Normalized capture width

FIGURE 8: Comparison between RAO and normalized capture width of the IPVA-PTO and the linear system for $\xi_e = 0.115$ (other parameters are shown in table 1)

bility demonstration project". *Electric Power Research Institute Inc*.

[3] Today, O. E., 27 March, 2019. "eni's new wave power device to convert mature offshore platforms into renewable energy hubs,". Accessed: January 31, 2021.

[4] Oliveira-Pinto, S., Rosa-Santos, P., and Taveira-Pinto, F., 2019. "Electricity supply to offshore oil and gas platforms from renewable ocean wave energy: Overview and case study analysis". *Energy Conversion and Management,* **186**, pp. 556–569.

[5] Bull, A. S., and Love, M. S., 2019. "Worldwide oil and gas platform decommissioning: a review of practices and reefing options". *Ocean & coastal management,* **168**, pp. 274–306.

[6] Jonkman, J., Butterfield, S., Musial, W., and Scott, G., 2009. Definition of a 5-mw reference wind turbine for offshore system development. Tech. rep., National Renewable Energy Lab.(NREL), Golden, CO (United States).

[7] Bureau of Safety and Environmental Enforcement, FEB, 2021. "platform structures online query,". Accessed: February 1, 2021.

[8] Babarit, A., Hals, J., Muliawan, M. J., Kurniawan, A., Moan, T., and Krokstad, J., 2012. "Numerical benchmarking study of a selection of wave energy converters". *Renewable energy,* **41**, pp. 44–63.

[9] Muliawan, M. J., Karimirad, M., and Moan, T., 2013. "Dynamic response and power performance of a combined spar-type floating wind turbine and coaxial floating wave energy converter". *Renewable Energy,* **50**, pp. 47–57.

[10] Karimirad, M., and Koushan, K., 2016. "Windwec: Combining wind and wave energy inspired by hywind and wavestar". In 2016 IEEE International Conference on Renewable Energy Research and Applications (ICRERA), IEEE, pp. 96–101.

[11] Cheng, Z., Wen, T. R., Ong, M. C., and Wang, K., 2019. "Power performance and dynamic responses of a combined floating vertical axis wind turbine and wave energy converter concept". *Energy,* **171**, pp. 190–204.

[12] Michailides, C., 2021. "Hydrodynamic response and produced power of a combined structure consisting of a spar and heaving type wave energy converters". *Energies,* **14**(1), p. 225.

[13] Babarit, A., 2015. "A database of capture width ratio of wave energy converters". *Renewable Energy,* **80**, pp. 610–628.

[14] Wan, L., Gao, Z., and Moan, T., 2015. "Experimental and numerical study of hydrodynamic responses of a combined wind and wave energy converter concept in survival modes". *Coastal Engineering,* **104**, pp. 151–169.

[15] Suzuki, H., and Sato, A., 2007. "Load on turbine blade induced by motion of floating platform and design requirement for the platform". In International Conference on Offshore Mechanics and Arctic Engineering, Vol. 42711, pp. 519–525.

[16] Yue, M., Liu, Q., Li, C., Ding, Q., Cheng, S., and Zhu, H., 2020. "Effects of heave plate on dynamic response of floating wind turbine spar platform under the coupling effect of wind and wave". *Ocean Engineering,* **201**, p. 107103.

[17] Koo, B., Kim, M., and Randall, R., 2004. "Mathieu instability of a spar platform with mooring and risers". *Ocean engineering,* **31**(17-18), pp. 2175–2208.

[18] Subbulakshmi, A., and Sundaravadivelu, R., 2016. "Heave damping of spar platform for offshore wind turbine with heave plate". *Ocean Engineering,* **121**, pp. 24–36.

[19] Liang, C., 2016. "On the dynamics and design of a wave energy converter with mechanical motion rectifier". PhD thesis, State University of New York at Stony Brook.

[20] Gupta, A., and Tai, W.-C., 2022. "The response of an inerter-based dynamic vibration absorber with a parametrically excited centrifugal pendulum". *Journal of Vibration and Acoustics*, pp. 1–39.

[21] Khasawneh, M. A., and Daqaq, M. F., 2021. "Internally-resonant broadband point wave energy absorber". *Energy Conversion and Management,* **247**, p. 114751.
[22] Khasawneh, M. A., and Daqaq, M. F., 2021. "An internally resonant tunable generator for wave energy harvesting". In Advances in Nonlinear Dynamics: Proceedings of the Second International Nonlinear Dynamics Conference (NODYCON 2021), Volume 3, Springer, pp. 233–239.
[23] Gao, Z., Moan, T., Wan, L., and Michailides, C., 2016. "Comparative numerical and experimental study of two combined wind and wave energy concepts". *Journal of Ocean Engineering and Science,* **1**(1), pp. 36–51.
[24] Mérigaud, A., 2018. "A harmonic balance framework for the numerical simulation of non-linear wave energy converter models in random seas". PhD thesis, National University of Ireland, Maynooth (Ireland).
[25] Cummins, W., Iiuhl, W., and Uinm, A., 1962. "The impulse response function and ship motions".
[26] Ogilvie, T. F., 1964. "Recent progress toward the understanding and prediction of ship motions". In 5th ONR Symp. on Naval Hydrodynamics.
[27] Gupta, A., and Tai, W.-C., 2022. "Ocean wave energy conversion of a spar platform using a nonlinear inerter pendulum vibration absorber". In International Design Engineering Technical Conferences and Computers and Information in Engineering Conference, Vol. 86311, American Society of Mechanical Engineers, p. V010T10A013.
[28] Beatty, S. J., Hall, M., Buckham, B. J., Wild, P., and Bocking, B., 2015. "Experimental and numerical comparisons of self-reacting point absorber wave energy converters in regular waves". *Ocean Engineering,* **104**, pp. 370–386.
[29] Seebai, T., and Sundaravadivelu, R., 2011. "Dynamic analysis of slack moored spar platform with 5 mw wind turbine". *Ocean Systems Engineering,* **1**(4), pp. 285–296.
[30] Kristiansen, E., Hjulstad, Å., and Egeland, O., 2005. "State-space representation of radiation forces in time-domain vessel models". *Ocean Engineering,* **32**(17-18), pp. 2195–2216.